Hybrid-Organic Photonic Structures for Light Emission Modification

Valentina Robbiano, Francesco Di Stasio, Salvatore Surdo, Shabbir Mian, Giuseppe Barillaro, and Franco Cacialli

Abstract We report the modification of the photoluminescence (PL) and decay rates of two different green-emitting conjugated polymers incorporated into photonic crystals with the stop-bands spectrally tuned on their emission. We observe both suppression (in the stop-band) and enhancement (at the high-energy band-edge) of the photoluminescence. Time-resolved measurements also reveal a concomitant modification of the emission lifetime that is enhanced at the band-edge and suppressed within the stop-band, thus confirming a variation of the radiative decay rate of the excitations in such photonic nanostructures. We propose two examples of fluorescent photonic composite systems. The first consists of a hybrid Si-organic system, obtained by infiltration of the polymer inside a rugate filter (a 1D photonic crystal). The second example is a fully organic system obtained by self-assembling of solvent-compatible microspheres-polymer system for obtaining a synthetic opal (a 3D photonic crystal) with a uniform distribution of the emitting material across the photonic structure.

Keywords 1D photonic crystals • 3D photonic crystals • Conjugated polymers • Conjugated polyrotaxanes • Functional materials @ photonic crystals • Hybrid photonic crystals • Light emission • Opal • Photoluminescence • Photophysics • Purcell effect • Rugate filters • Self-assembly • Silicon • Spontaneous emission

V. Robbiano • F. Cacialli (✉)
Department of Physics and Astronomy and London Centre for Nanotechnology, University College London, Gower Street, WC1E 6BT London, UK
e-mail: valentina.robbiano.12@ucl.ac.uk; f.cacialli@ucl.ac.uk

F. Di Stasio
Nanochemistry Department, Istituto Italiano di Tecnologia, Via Morego 30, 16163 Genoa, Italy
e-mail: francesco.distasio@iit.it

S. Surdo • G. Barillaro
Dipartimento di Ingegneria dell'Informazione, Università di Pisa, Via Diotisalvi 2, 56122 Pisa, Italy
e-mail: Salvatore.Surdo@iit.it; g.barillaro@iet.unipi.it

S. Mian
Department of Physics, McDaniel College, Westminster, MD 21157, USA
e-mail: smian@mcdaniel.edu

D. Comoretto (ed.), *Organic and Hybrid Photonic Crystals*,
DOI 10.1007/978-3-319-16580-6_15

1 Introduction

In the last 30 years, there has been an increasing interest in the development of novel photonic structures to control the light-emission properties of materials, as well as for the fabrication of semiconductor lasers. The concept of a photonic crystal (PhC) was introduced in 1987 with the studies of Yablonovitch [1] and John [2] on the inhibition of the spontaneous emission and light localization effects. These relate to structures whose periodicity in refractive index would enable to control, suppress, or enhance the propagation of photons, in analogy with the already well-established possibility to control electron propagation in "electronic" crystals, in which the periodicity of the electronic potential results in allowed and forbidden energy bands for the electrons. As well-described by Joannopolous and collaborators in their book [3], this is due to the possibility to re-write Maxwell equations in terms of a single master equation, in which the dielectric function plays a similar role to the potential in Schrödinger's equation. The field of photonic structures and crystals has then developed in a variety of directions, often dictated by the hurdles of fabrication of structures whose periodicity needs to be on the same lengthscale as that of the wavelength of the light one desires to control. This places some stringent requirements for PhCs that need to operate in the visible range, as one needs to generate photonically active patterns with typical dimensions/periodicities of the order of a few hundreds of nanometres. So far, the development and production of photonic crystals has been generally focused on top-down nanofabrication [4–7] making use of lithographic techniques such as electron-beam and focused ion-beam patterning (FIB). These are very expensive, and being essentially "serial" suffer from significant limitations in terms of either surface areas or sample throughput, in addition to being limited to the fabrication of mainly two-dimensional structures. Another major drawback is that the photonic effects are strongly inhibited by the residual surface roughness, thus spoiling the overall Q-factor of the cavities [8]. One technique that has shown more promise is the laser-assisted photopolymerization/activation of a cross-linker, to generate 3D nanostructures [9, 10] but for the as-prepared structures one needs some extremely careful control of relaxation effects of the structures after the polymerization to avoid distortion of the architectures and to ensure adherence to the intended pattern. By contrast, bottom-up approaches exploit the collective self-assembly of suitably sized building blocks (typically colloidal dielectric microspheres). This provides a much easier, faster and low cost alternative to top-down methods in preparing photonic crystals, enabling the preparation of both 2D (close-packed microspheres monolayers [11, 12]) and, more interestingly, 3D (artificial opals [13–16] and inverse opals [17, 18]) structures. Concerning opals and inverse opals, you could also read the chapter by C. López et al., in this volume. Since this is not a "serial" approach, it has the scope and potential to generate significantly larger samples. However, self-assembly methods lead to structures with a relatively high density of defects [19] that limit their application in optical devices. In addition, and somewhat in between the two approaches detailed above, we find a host of

"non-conventional" top-down methods that are not "serial" (as e-beam and FIB) thereby allowing fabrication of structures over large (several square cm) areas. These methods consist, for example, in the spin-coating of polymers [20, 21] and the electrochemical micromachining of porous silicon [22–24]. Whereas spin-coating has been mainly used just to fabricate polymeric multilayers (e.g. full-plastic distributed Bragg reflectors), electrochemical micromachining, that consists of a controlled electrochemical etching of porous silicon, is a far more versatile technique and enables the preparation of inorganic PhCs with different dimensionalities (1D rugate filters and 2D arrays) with sub-micrometre accuracy [25, 26].

Photonic crystals exhibit a variety of optical properties that can be exploited in a variety of optoelectronics applications, such as optical fibres [27], sensors [28], solar cells [29] (see the chapter by Marina Mariano et al., in this volume), light-emitting diodes [30] and lasers [31]. In particular, PhCs are a fundamental component of laser sources, since they are necessary to provide optical feedback to the gain medium. For lasing application, see also the chapter by Seiichi Furumi, in this volume. A notable example of a laser based on a complex PhC structure is the work of Painter et al. where [32] controlled structural defects lead to the formation of optical microcavities with extremely high finesse, thus enabling laser emission from an embedded gain material with a very low stimulated emission threshold [21, 32]. An important property of PhCs is their ability to control the spontaneous emission of an embedded light-emitting material. The emission modification phenomena induced by PhCs are also reported in the chapters by L.C. Andreani and M Liscidini; F. Scotognella et al.; and Pieter-Jan Demeyer and Koen Clays, in this volume. In fact, the photonic band gap of a PhC can either inhibit or enhance spontaneous emission by modifying its radiative rate. When an active material is embedded into a PhC, its optical properties are strongly affected by the periodical dielectric environment, which alter the dispersion properties of photons (i.e. photonic density of states, p-DOS) [33]. Indeed, the p-DOS diminishes within the photonic band gap thus suppressing light-emission. On the other hand, at the edges of the photonic band gap, the p-DOS increases [34], i.e. a light-emission enhancement is observed. Both enhancement and suppression of the emitted light are accompanied by an increase and decrease of the radiative rate, respectively. Such an effect on the radiative rate can be used to modify, for example, the photoluminescence spectrum and intensity of the embedded material. In addition, the cross section of stimulated emission directly depends upon the radiative rate of the material. Therefore, increasing the radiative rate directly decreases the stimulated emission threshold.

To study the control of light, as well as to fabricate a variety of laser structures, conjugated polymers have been widely used as emitting materials. This is mainly due to their versatile processing, wide colour tunability (from NIR to near UV), high solid-state photoluminescence efficiency and strong optical absorption (up to $\sim 10^5$ cm^{-1}) [35, 36]. Furthermore, both conjugated molecules and polymers demonstrate low stimulated emission threshold [37–40] since they are an intrinsic four-level system [41], making them a promising gain material for the fabrication of solution processable semiconductor lasers in combination with hybrid and

organic PhCs. The first optically pumped laser incorporating a neat conjugated polymer has been reported by Tessler et al. [31]. In this work, the authors studied the emission of poly(*p*-phenylene vinylene), PPV, prepared inside an optical cavity formed by a distributed Bragg reflector (DBR) and a silver mirror. Such photonic structures are relatively easily fabricated, but offer no lateral confinement and can support several in-plane modes causing optical losses. The most studied class of PhCs in the organic photonics field are distributed feedback (DFB) lasers [42, 43]. These devices consist of an active material film (in our case a conjugated polymer) deposited onto a corrugated substrate, which provide optical feedback by confining the light "in plane", similar to a waveguide. Many other configurations have been exploited for organic semiconductor lasers: flexible microcavities [21, 44], block-copolymer DBRs [45], opals [46], inverse opals [47] and opals microcavities [48, 49] infiltrated with dyes, random structures [50] and 2D photonic structures [7, 51].

Despite the numerous types of PhCs used, electrically pumped lasing has not been achieved yet, to the best of our knowledge, in conjugated polymer-based system. Restricting our discussion to these as gain materials, the main limitations that we can identify relate to (1) PL quenching by interchain interactions, [52] (2) polaron [53] and triplet absorption [54] (particularly severe for electrical pumping given that spin statistics strongly favour formation of triplets over singlets), (3) losses at the metallic electrodes (in the case of injection lasers) [55], (4) limited charge mobility [56] (preventing suitably large pumping current for injection lasers), and (5) material degradation under optical and electrical pumping [57]. Whereas several synthetic approaches have been used to reduce π–π stacking, increase distances between polymer chains [58] and reduce crystallinity [59]; for example by attaching side-groups to the conjugated backbone [60] or by threading the conjugated chain with molecular rings that act as spacers (i.e. as in polyrotaxanes) [61], significant progress is still needed to overcome the other limitations above. In general, both novel PhCs and conjugated polymers need to be developed and investigated to achieve CW optically pumped or electrically pumped lasing and in the following we report two examples from our experience in which we observed emission modification of two different conjugated polymers embedded into photonic crystals. The first system consists of 1D silicon PhCs, a rugate filter, where the luminescent polymer is infiltrated via dip-coating; the second one is a 3D PhC (synthetic opals) where the conjugated polymer is embedded into it. Such photonic structures enable emission modification of the conjugated polymers. In fact, we observed both suppression (in the stop-band) and enhancement (at the high-energy band-edge) of the photoluminescence. Remarkably, time-resolved measurements reveal a modification of the emission lifetime, which is enhanced at the band-edge and suppressed within the stop-band, and clearly point to a variation of the radiative decay rate of excitations in such hybrid-organic photonic nanostructures.

2 Hybrid Inorganic–Organic Photonic Structures: Rugate Filters Infiltrated with Polyfluorene Derivative

Porous silicon-based PhCs, such as rugate filters [62], have attracted significant interest since they provide a technologically robust route to fabrication of optical nanostructures with significant levels of complexity. Indeed, this class of photonic systems has been used widely for optoelectronic [63], photonic [64], sensing [28] and biological applications [65]. In particular, rugate filters are good candidates as vapour and liquid sensors [66–68], and as detectors for biological activities such as proteases [69, 70]. However, preparation of hybrid Si-organic structures, where an organic material is infiltrated into the pores of the rugate filter is not always straightforward, especially when pore sizes are comparable to the polymers gyration radii, or to the size of aggregated/phase-separated macromolecular mesostructures, thus causing pore clogging which often prevents complete infiltration [71]. One way to infiltrate macro-molecules inside the photonic structure is to grow the molecules "in situ" inside the pores starting from smaller monomers [72], via either electrochemical deposition [73, 74] or in situ chemical polymerisation [75]. The major drawback of this methodology is the intrinsic limitation to a relatively narrow set of monomers, and therefore not generally satisfactory. Interestingly, the particular ratio between the limited gyration radius (R_g, of the order of few nm) of poly[(9,9-di-*n*-octylfluorenyl-2,7-diyl)-alt-(benzo[2,1,3]thiadiazol-4,8-diyl)], (F8BT, Mw ~46 kDa) and the minimum pore sizes (approximately 10 times larger than R_g) allowed us to infiltrate the polymer inside the pores. In fact, we observe shifts of the reflectance peaks of the structures consistent with coating of the inner walls of the pores to the whole depth that can be probed in such optical experiments. Porous silicon rugate filters were prepared by electrochemical etching of (100)-oriented, highly boron doped p-type silicon wafers in a 3:1 (by vol.) solution of 48 % (by vol.) aqueous hydrofluoric acid and ethanol. The electrochemical etching was performed using a two-electrode configuration, with the silicon substrate acting as anode (working electrode) and a platinum ring immersed in the solution acting as cathode (and used as pseudo-reference electrode). A cosine-shaped current density waveform with peak-to-peak dynamics from 13.3 to 39.9 mA cm^{-2}, 50 repeats, and time period of 11 and 17.5 s was used to produce rugate filters with a stop-band in reflectance centred at 551 and 875 nm, respectively. The resulting porous silicon structures possess sinusoidally shaped periodic cavities with porosity values (defined as the ratio between the mass of etched silicon with respect to the total silicon subjected to etching) between 55.3 and 62.3 %; and a sinusoidally shaped refractive index as well, which varies between 1.95 and 2.21. To improve the infiltration process and prevent emission quenching from the heavily doped silicon layer, the rugate filters were partially oxidized into a tube furnace under pure-O_2 at 600 °C for 30 min. The oxidation leads to a general decrease of the effective refractive index of the rugate filter and, in turn, in a blue-shift of the stop-band to 515 nm (from 551 nm) and 771 nm (from 875 nm). Figure 1 shows Scanning Electron Microscope images at different magnification of one of

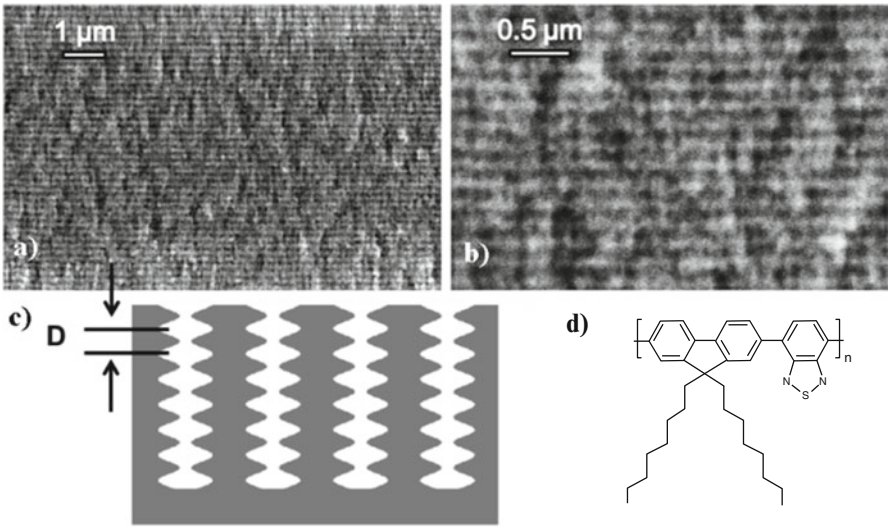

Fig. 1 (**a**, **b**) SEM cross sections at different magnifications of an as-prepared porous silicon rugate filter with resonant peak in reflectance centred at 875 nm. (**c**) Scheme of the cross section in (**a**) and (**b**) of the as-prepared rugate filter. *D* is the inter-planar spacing that is determined by the preparation conditions. (**d**) Chemical structure of F8BT

the as-prepared rugate filters and a scheme showing the same cross section. The size of pores is in the range of 80–100 nm for both structures, and the inter-planar spacing D is around 100 and 200 nm for the rugate filters with stop-band at 551 and 875 nm (before oxidation), respectively.

The F8BT was dissolved in a toluene solution 1 mg/ml, stirred overnight at room temperature and then filtered. The infiltration was obtained via dip-coating carried out at a controlled lifting rate (0.01 mm/min) and temperature (29 °C) inside an incubator. The excess polymer layer left onto the surface after dip-coating was removed using a cotton swab soaked with toluene. We consider that this procedure might have also helped the polymer infiltration. To assess the effect of the photonic structure on the F8BT spectrum, we compared the rugate whose stop-band is centred at 515, thus spectrally overlapping (i.e. tuned with the F8BT PL spectrum) with the rugate whose stop-band is centred at 771 nm and hence detuned with respect to the F8BT PL spectrum. The latter is used as reference to observe any PL modifications induced by the presence of the PhC since F8BT film has the same morphology as the one infiltrated into the tuned one.

Figure 2 shows the reflectance spectra for tuned and detuned samples before and after the infiltration of the F8BT and the typical PL spectrum of an F8BT film. Upon polymer infiltration, the reflectance peaks red-shifted by ~12 nm in both samples due to the increased effective refractive index of the F8BT with respect to air. In particular the reflectance peak for the tuned sample red-shifted from 515 to 528 nm

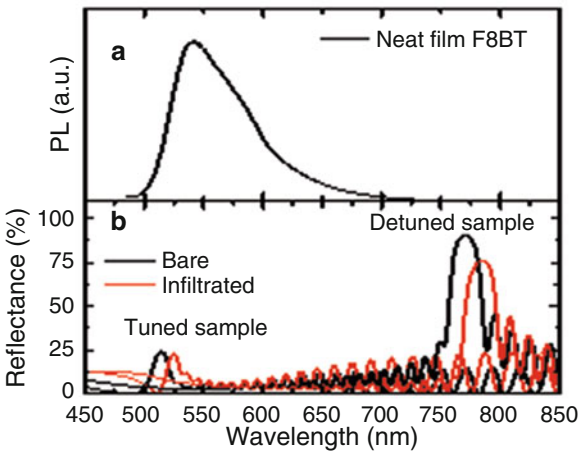

Fig. 2 (**a**) PL spectrum of a neat film of F8BT and (**b**) Reflectance spectra for the PhCs before (*black*) and after polymer infiltration (*grey*). The infiltration leads to a red-shift of the photonic stop-band (and thus of the reflectance peak)

after infiltration and for the detuned one it red-shifted from 771 to 784 nm. This is predicted by the Bragg–Snell law [76]:

$$m\lambda = 2D\sqrt{n_{\text{eff}}^2 - \sin^2\theta} \tag{1}$$

where m is the diffraction order, λ the spectral position of the stop-band peak, n_{eff} the effective refractive index of the photonic crystal, θ the incidence angle and D the inter-planar spacing, that is determined by the preparation condition. The effective refractive index can be calculated by using the Lorentz–Lorenz equation and depends on the refractive indices of the media composing the PhC (in this case silicon, silicon dioxide and air before infiltration, and silicon, silicon dioxide, and F8BT after) weighted by their volume fraction.

$$\frac{n_{\text{eff}}^2 - 1}{n_{\text{eff}}^2 + 2} = \sum\nolimits_{\text{media}} f_{\text{medium}} \frac{n_{\text{medium}}^2 - 1}{n_{\text{medium}}^2 + 2} \tag{2}$$

where f is the volume fraction for each media.

Considering that the refractive indices of F8BT are 1.6 (extraordinary one) and 1.8 (ordinary one) [77] and the refractive index of air is 1, if the cavities have been completely filled by the polymer, according to Lorentz–Lorenz equation, a spectral shift of the reflectance peaks bigger than the one that observed from the measured spectra is expected. By analysing the reflectance peaks spectral shifts, it can be assumed that in this case the effective refractive index is not just a combination of the refractive indices of Si and F8BT and therefore the polymer does not entirely fill the nanostructured cavities. In fact, in this experiment, the infiltration consisted in the deposition of thin polymer films on the walls of the cavities. In this case, the final effective refractive index would be the combination of the ones of the silicon, silicon dioxide F8BT and air. It is reasonable to exclude a partial filling of

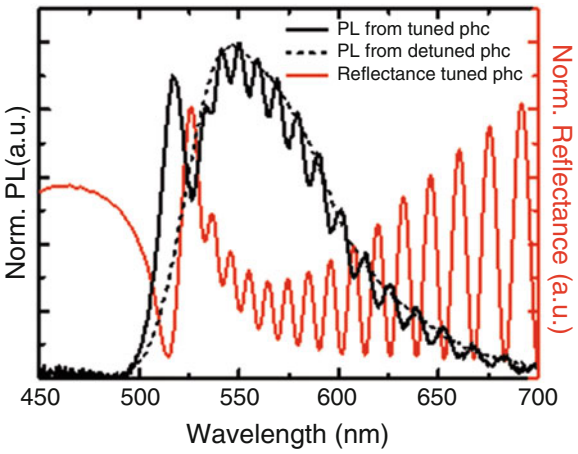

Fig. 3 PL spectra collected at normal incidence (0^o) of the exciting beam for F8BT infiltrated into the tuned PhC (*solid line*) and for the F8BT infiltrated into the detuned PhC (*dashed line*). Reflectance spectrum (*grey line*) of the tuned PhC is shown

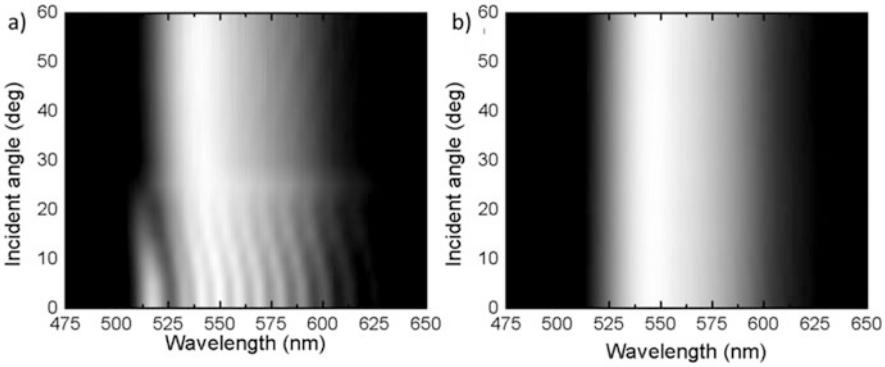

Fig. 4 Contour plots of the PL spectra as a function of the incidence angle for the F8BT infiltrated into the tuned (**a**) and detuned (**b**) PhC

the cavities due to the presence of just one reflectance peak, otherwise it would have been observed two reflectance peaks for the two PhCs stacking one over the other (i.e. the one made by Si and air and the one made by Si and polymer [78]).

To observe PL modification induced by the photonic crystal, PL measurements have been carried out both from the F8BT infiltrated into the tuned and detuned rugate filters; the second one has been used as reference. The PL spectra collected at normal incidence of the F8BT infiltrated into both rugate filters are shown in Fig. 3, together with the reflectance spectrum of the tuned rugate filter. Remarkably, the PL spectrum of F8BT is strongly modified by the optical features of the rugate filter: both the photonic stop-band and the interference fringes. In particular, the photonic band gap (PBG) partially suppresses light propagation at 527 nm and it also induces an increase in the PL intensity in the PBG high-energy edge. Interestingly, also the diffraction fringes modify the emission, leading to a sinusoidal modulation of the PL spectrum. In Fig. 4 we report the contour plot of the PL spectra as a function of

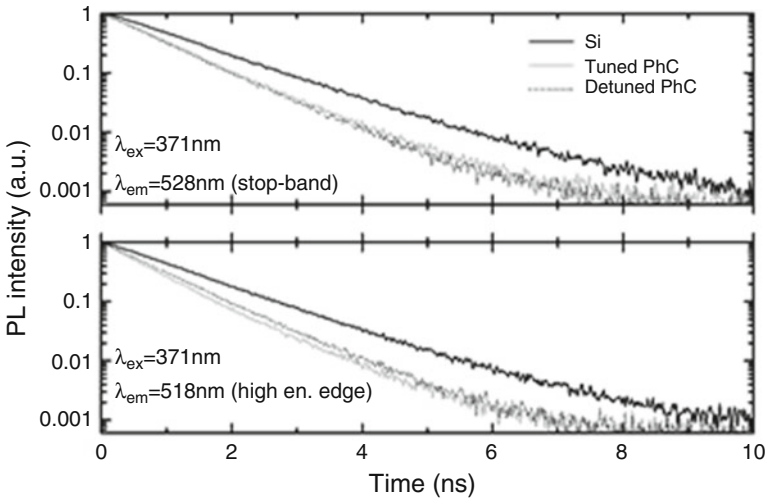

Fig. 5 Radiative decay of F8BT PL recorded at the stop-band (528 nm, *top panel*) and at the high-energy edge (518 nm, *bottom panel*). The measurement shown here was collected for the F8BT infiltrated into the tuned and detuned crystals (*grey solid line* and *black dashed lines*, respectively) and for a neat film of F8BT over a Silicon substrates (*black solid line*)

the angle of incidence of the laser beam for the F8BT infiltrated into the tuned PhC and detuned PhC. As expected, both the enhancement and the suppression are angle dependent because of the dispersion of the stop-band.

Final investigation consisted in the evaluation of the radiative decay of the F8BT PL (Fig. 5) both in the PBG (528 nm) and at the high-energy edge of the stop-band (518 nm). We focused on these two spectral lines because at such wavelengths there is a clear modification of the photonic density of state (p-DOS), as demonstrated by the reflectance spectra. In particular in the PBG there is a suppression of the photonic density of states, whereas at the high-energy edge of the stop-band the p-DOS is increased [33].

In previous studies the PL decay for neat film of F8BT deposited by spin-coating has been reported with a mono-exponential equation [79] with fluorescence decay lifetime varying from 0.89 to 1.4 nm depending on the wavelength, film thickness and substrate materials [80, 81]. In our case, for a neat film (thickness ~800 nm) on Si deposited by dip-coating, we obtained analogous values (1.15 ns at 518 nm and 1.18 ns at 528 nm, Table 1). Interestingly, we observed that when the polymer is infiltrated both in the tuned and detuned PhCs, the PL decay can be fitted with a double exponential expression:

$$I(t) = I_0 + I_1 e^{-\left(t/\tau_1\right)} + I_2 e^{-\left(t/\tau_2\right)} \tag{3}$$

The lifetimes (τ_1 and τ_2) used in the fit-curves of the temporal evolution of the PL of the F8BT infiltrated into the crystals are reported in Table 1. The presence of

Table 1 Lifetime values (τ_1 and τ_2) extrapolated from the fit-curves of the PL decay

	$\tau_1(I_1)$	$\tau_2(I_2)$
High-energy edge (518 nm)		
PhC	690 ± 34 ps (0.8)	1,210 ± 60 ps (0.2)
Detuned	830 ± 41 ps (0.95)	1,590 ± 79 ps (0.05)
Film	1,150 ± 57 ps	
Stop-band (528 nm)		
PhC	860 ± 43 ps (0.94)	1,680 ± 84 ps (0.06)
Detuned	830 ± 41 ps (0.95)	1,600 ± 80 ps (0.05)
Film	1,180 ± 59 ps	

I_1 and I_2 indicate the relative contribute of each time constant. We estimated an error of 5 % on the measured value

a bi-exponential decay instead of a single exponential one can be attributed to a stronger interaction of the polymer with the Si substrate when inserted into the cavities. In fact, in this configuration the polymer layer is thinner compared to the neat film onto flat Si substrates. At the high-energy edge of the stop-band (518 nm), the decay for the F8BT infiltrated into the tuned rugate filter is faster than for the reference (i.e. the F8BT infiltrated into the detuned rugate filter) by ~17 % from the weighted mean of τ_1 and ~24 % τ_2 (Table 1), whereas within the stop-band (528 nm) the reverse situation occurs and the lifetimes are longer in the tuned sample compared to the detuned. Although these differences between the radiative decay rates [109] of the F8BT are relatively small, it should be considered that the photonic confinement for such samples happens only along the z-direction and that the rugate filter we have worked with had a narrow spectral width (516–533 nm) compared to the PL spectrum of F8BT (490–700 nm) [34].

3 Colloidal Photonic Crystals Self-assembled with Water-Soluble Conjugated Polyrotaxanes

Colloidal self-assembled PhCs represent another class of photonic structures that can be easily combined with conjugated polymers. Within self-assembled PhCs, synthetic opals [1, 2, 82, 83] have been especially popular thanks to their low cost of fabrication and ease of preparation. Furthermore, their functionalization with light-emitting materials can be easily achieved via infiltration by vapour phases [84], or solutions [82], allowing the investigation of a variety of photonic effects [85], including the modification of the emission spectra and radiative rates [34, 86]. Various materials such as metal nanoparticles [87], semiconductor nanocrystals [88] or conjugated molecules [89] have been incorporated into synthetic opals via infiltration. Nevertheless, achieving a homogenous distribution of the active materials in the opal via infiltration still represents a major challenge. To overcome this issue many fabrication techniques have been proposed, as, for example, infiltration of monomers followed by in situ polymerization [90], or layer-by-layer polymer

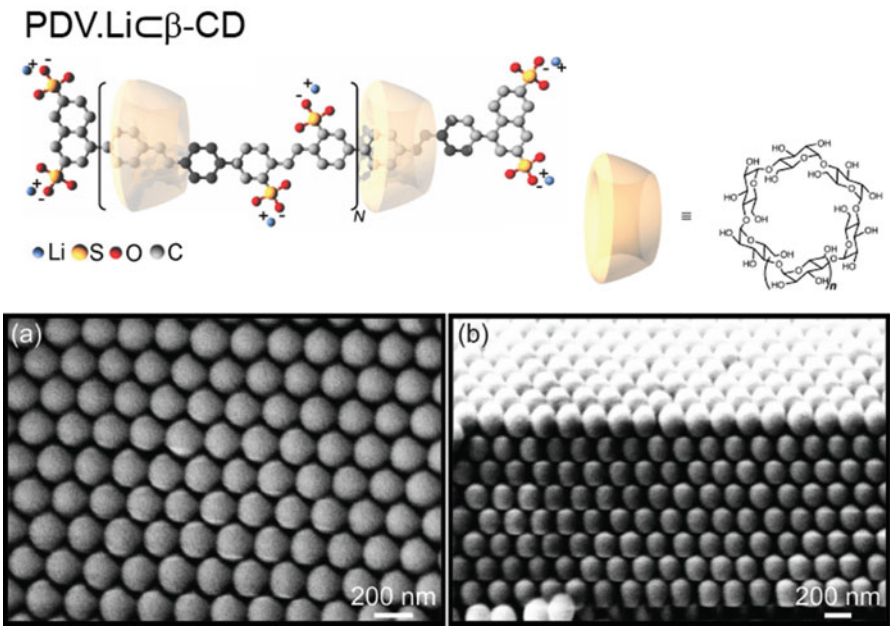

Fig. 6 *Top*: Chemical structure of PDV.Li⊂β-CD, threading ratio = 2, with an average number of repeat units $n = 10$. *Bottom*: SEM micrographs of an opal film incorporating PDV.Li⊂β-CD: (**a**) cryo-cleaved wall surface showing the internal structure of the opal, (**b**) film cross section. Strong contrast between the sphere and the interstices is observed, confirming that the latter are not filled up by the conjugated polyelectrolytes (the density of the conjugated moiety and of the spheres being comparable). Reproduced and adapted with permission from [98]

coating of the sphere surfaces [79]. Water-soluble conjugated polymers can be directly incorporated into the synthetic opal during growth, allowing for a "one-pot" chemical approach which does not require further sophisticated fabrication techniques. To this end, conjugated polyelectrolytic rotaxanes [58] (Fig. 6) are a well-suited class of materials for incorporation into synthetic opals since they demonstrate high photoluminescence quantum yield. Conjugated polyrotaxanes are supramolecular architecture in which a conjugated backbone, such as poly (4,4′-diphenylene vinylene) (PDV), is threaded through cyclodextrin rings (β-CD), that sterically impose increased inter-molecular distances. Such structures lead to higher photoluminescence quantum yield and reduced polaron formation compared to unthreaded materials [91], thus enabling optically pumped lasing [92], optical amplification [93] and fabrication of white-emitting organic light-emitting diodes [94, 95].

Opal films can be prepared using commercially available aqueous suspensions of monodisperse polystyrene nanospheres [96] (standard deviation < 5 %; refractive index, $n_{PS} = 1.59$), that can be diluted in de-ionized water as necessary to obtain the desired film thickness ($d \sim 5$ μm) upon complete water evaporation. β-CD-threaded PDV (PDV.Li⊂β-CD) was used as water-soluble luminescent semiconductor.

PDV.Li⊂β-CD is a polyelectrolytic derivative of poly-*para*-phenylene vinylene (PPV) where sulfonate side-groups balanced by Li^+ ions afford solubility in polar solvents (molecular structure in Fig. 6) [89, 97]. PDV.Li⊂β-CD incorporation was carried out by dissolving it in water, and then adding the solution to the nanospheres water-suspension before proceeding with the PhC growth process inside an incubator. To ensure that the presence of the polyrotaxane does not negatively affect the growth of the PhC, concentrations for the polyrotaxane water solutions ranging from 0.5 mg/ml to 1×10^{-3} mg/ml were investigated. The PhCs here discussed were prepared using a PDV.Li⊂β-CD concentration of 8×10^{-3} mg/ml which yielded undistorted, homogenous opals without deposition of an excess polymer layer on their surface, while preserving strong PL properties of the system.

The growth process was carried out at 45 ± 1 °C on soda-lime glass slides using the meniscus technique [89, 96, 99], thus obtaining a face-centred cubic lattice of nanospheres with the [110] direction perpendicular to the substrate. The obtained PhCs had an area of $\sim 7 \times 7$ mm^2. Scanning electron microscopy (SEM) micrographs (Fig. 6a, b) of the co-grown opal show no presence of lattice distortion induced by the incorporation of polyrotaxanes, nor an excess polymer layer on the opal surface for PhCs with 8×10^{-3} mg/ml PDV.Li⊂β-CD solution. Moreover, the interstices between nanospheres are empty, thereby preserving a desirable higher dielectric contrast within the structure than otherwise possible in case of substantial filling of the interstices. Preservation of the opal structure and optical properties upon polyrotaxane incorporation is demonstrated by the presence in reflectance spectra (Fig. 7a at wavelengths near and below 300 nm) of van Hove-like structures [100]. These features are due to diffraction along directions different from the incident one [33, 100] and are known to depend strongly on the order of

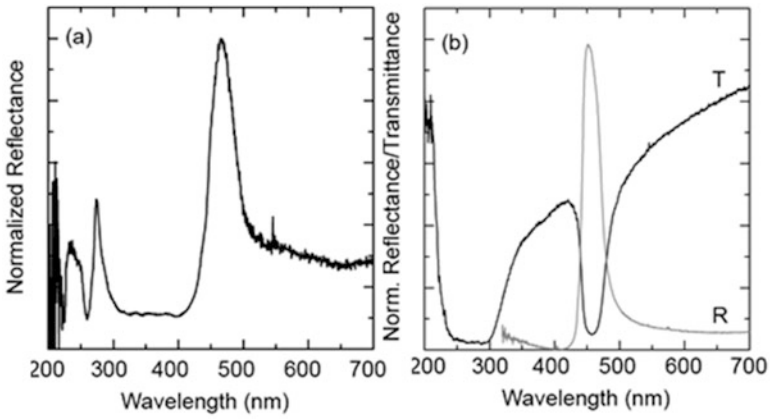

Fig. 7 (**a**) Reflectance spectrum of a typical co-grown opal with PDV.Li⊂β-CD fabricated with 200 nm polystyrene nanospheres showing van-Hove-like structures below 300 nm. (**b**) Reflectance (R) and transmittance (T) spectra of a polystyrene opal film co-grown with PDV.Li⊂β-CD (sphere diameter $a = 200$ nm, refractive index, $n_{PS} = 1.59$). The full-width-half-maximum of the PBG is not affected by the incorporation process. Reproduced and adapted with permission from [98]

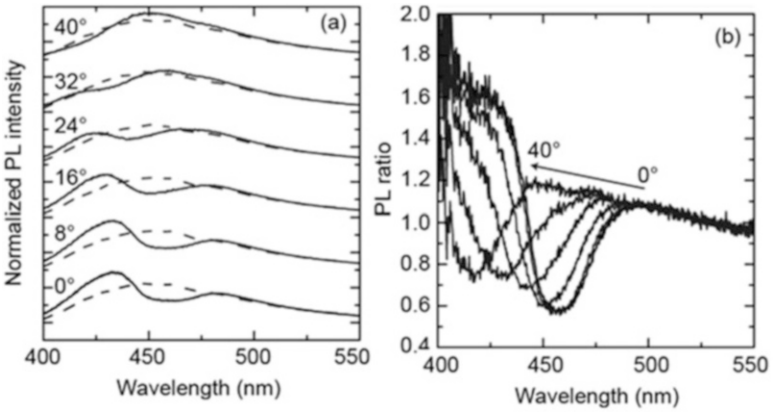

Fig. 8 (**a**) PL spectra of an opal film co-grown with PDV.Li⊂*β*-CD before (*solid line*) and after (*dashed line*) the thermal treatment at 75 °C at different incidence angle of the exciting beam [106], (**b**) ratio between the two PL spectra before and after the thermal process. In both panels the detection angle has been increased up to 40° with steps of 8°. Adapted and reproduced with permission from [98]

the system [33, 100–102], the microsphere quality [102], and the degree of incorporation of the luminescent material [84–87, 89, 103]. Indeed, they disappear when the structure is not enough regular, or when strongly absorbing materials are incorporated. In the case of co-grown opals, van Hove-like structures can still be observed both in the reflectance spectra [100] (Fig. 7a). All these features, combined with the additional effect of the PBG on the PL spectra (see Fig. 8a), can only be compatible with a minor incorporation of the rotaxinated polymer within the opals, such that the opal optical properties are not affected.

Figure 7b shows reflectance (R) and transmittance (T) spectra of the co-grown opal made with polystyrene beads with diameter $a = 200$ nm used in this study. As expected, the peak of reflectance at 455 nm ($E_B = 2.74$ eV) corresponds to a minimum in the transmittance spectrum. Significant changes in the optical properties of the PBG of the PhC upon incorporation of the rotaxanes are not observed. Both the spectral position of the stop-band and its full width at half-maximum ($\Delta E_B = 0.16$ eV) are unchanged compared to a bare opal [89, 97, 99], once again confirming the lack of lattice distortion and dielectric contrast modification, as expected from the SEM micrographs [76, 87, 103]. As a reference sample to study PL modifications induced by the PhC, the very same opal was thermally annealed at 75 °C for 5 min. Thermal annealing at 75 °C is enough to partially melt the polystyrene spheres, and thus destroy any photonic property of the structure [104] (as proven by the PL spectrum in Fig. 8a), without affecting the PL properties of the conjugated polyrotaxane, thanks to the higher thermal stability of this class of supramolecular systems [105].

To be able to compare the different properties, both measurements were carried out in the same area of the sample before and after the thermal process and the PL spectra were normalized at $\lambda = 550$ nm, far away from the PBG [34, 86, 89].

Figure 8 displays the PL spectra as a function of the incidence angle of the excitation beam for the co-grown PhCs and the reference sample. A 50 nm blue-shift of the PL peak and a small increase of the PL quantum yield (Φ_{PL}) to 38 ± 3 % (for the melted-opal "reference" samples) compared to a neat spin-coated film of PDV.Li⊂β-CD ($\Phi_{PL} \sim 18 \pm 2$ %) is observed [58, 107]. The PL blue-shift and the variation of Φ_{PL} can be assigned to electrostatic interactions of the Li cations with the negatively charged surface of the polystyrene nanospheres. This interaction changes the polymer structure, i.e. the electronic structure of semiconducting chains close to the surface. Furthermore, the opal growth is mainly driven by capillary forces [96] that would also act on the polyrotaxanes and impose additional structural constraints, with a concomitant modification of the PL dynamics of the polyrotaxane with respect to a neat-polymer film or solution [91]. This interpretation is further supported by what previously observed for poly(phenylene-ethynylene) polyelectrolytes neat and grafted to silica microspheres, for which a spectral blue-shift has also been observed. The PL spectrum of PDV.Li⊂β-CD (Fig. 8a) is strongly modified by the PBG, which partially suppresses (up to 33 %) light propagation between 448 and 482 nm (at 0° incidence). Instead, an increase of the PL intensity is observed at the short-wavelength edge of the PBG. As expected, both the enhancement and the suppression depend on the detection angle [34, 89] according to the dispersion of the PBG, thus inducing a directionality to the observed effect. The enhancement/suppression effects caused by the PhC with respect to the "melted reference" can be made more obvious by plotting the ratio between the two PL spectra, as in Fig. 8b: within the PBG the ratio is <1, but >1 at the short-wavelength edge of the PBG [34, 88, 89, 108].

Time-resolved PL measurements at the relevant wavelengths, i.e. at 437 nm (PL enhancement) and at 460 nm (PL suppression, Fig. 9) give further insight into the underlying photophysics of these photonic structures. In previous studies, the

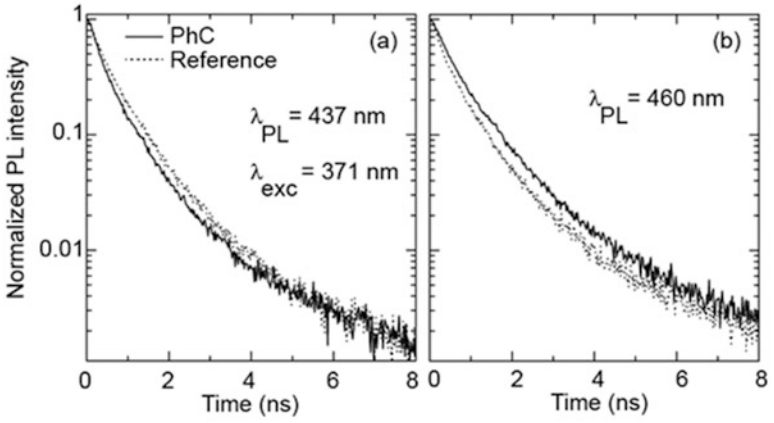

Fig. 9 Temporal evolution of the PDV.Li⊂β-CD PL measured at the short-wavelength edge (**a**, 437 nm) and inside (**b**, 460 nm) the PBG before (*solid line*) and after (*dashed line*) the thermal treatment at 75 °C. All measurements were carried out in air and at room temperature. Adapted and reproduced with permission from [98]

Table 2 Lifetime values (τ_1, τ_2, τ_3) used in the fit-curves the temporal evolution of the PL (the relative contribute of each time constant is included in parentheses)

	τ_1, ps (I_1)	τ_2, ps (I_2)	τ_3, ps (I_3)
437 nm (high-energy edge)			
PhC	300 ± 15 (0.33)	790 ± 40 (0.56)	2,720 ± 140 (0.11)
Reference	370 ± 20 (0.33)	860 ± 43 (0.57)	2,650 ± 130 (0.10)
460 nm (PBG)			
PhC	430 ± 20 (0.32)	950 ± 50 (0.55)	2,850 ± 140 (0.13)
Reference	365 ± 20 (0.34)	860 ± 40 (0.53)	2,750 ± 140 (0.13)

We estimated an error of 5 % on the measured value. Reproduced with permission from [98]

PL decay dynamics of polyrotaxane films have been fitted with a double exponential expression and assigned to the *intramolecular* singlet exciton and *inter*-molecular aggregate states [91]. Surprisingly, for the co-grown opal a triple-exponential expression: $I(t) = I_0 + I_1 e^{-\left(\frac{t}{\tau_1}\right)} + I_2 e^{-\left(\frac{t}{\tau_2}\right)} + I_3 e^{-\left(\frac{t}{\tau_3}\right)}$ must be used (Table 2). Whereas the longer decay times (τ_2 and τ_3), can be readily assigned to those previously identified ($\tau_{\text{exciton}} \sim 850$ ps, $\tau_{\text{aggregate states}} \sim 2{,}600$ ps) [91], the (fast) additional decay channel can be assigned to a new emissive species arising from the previously discussed interaction of the polyrotaxane with the nanospheres surfaces. This hypothesis is further supported by the observation of a three-exponential decay also in the annealed reference sample, suggesting that such a de-excitation pathway is observed only in the presence of polyrotaxane/colloid interaction. Furthermore, the weight of the different decay channels is similar at 437 and 460 nm for the PhC and the melted "reference". In addition, τ_3 is comparable in the opal, in the melted "reference" (2,650 ps at 437 nm and 2,750 ps at 460 nm) and in neat spin-coated films. At the short-wavelength edge of the stop-band (437 nm) the decay for the co-grown opal is shorter than for the reference (by 11 %, as estimated from the weighted mean of τ_1 and τ_2) whereas within the stop-band (460 nm) the reverse situation occurs (13 %, Table 2).

Indeed, a sizable effect on the radiative lifetime (Purcell effect) [109] can only be observed in photonic crystals for which the photonic density of states is strongly modified in the whole *k*-space. For synthetic polystyrene opals, the PBG is present only along the [110] (ΓL) crystallographic direction and it is spectrally narrow (447–482 nm) when compared to the width of the PL spectrum (405–650 nm), thus reducing the observable effect [34]. Furthermore, Φ_{PL} of PDV.Li⊂*β*-CD in the reference sample is ~38 ± 4 %, meaning that the radiative rate (K_{R}) is smaller than the non-radiative rate (K_{NR}), i.e. any modification caused by a redistribution of the photonic density of states will have a small effect on the PL lifetime. Interestingly, the observed PL lifetime modification is wavelength-dependent with a precise overlap with the PBG spectrum. According to this observation and previously reported experiments [34, 89] this effect can be assigned to the modification of the density of photonic states along the ΓL direction.

As a first order approximation, the modification of the PL lifetime can be considered as only induced by the redistribution of the photonic density of states,

thus allowing an estimate of the variation of K_R. If we consider Φ_{PL} as the sum of contributions of the three emissive species, we obtain:

$$\Phi_{PL} = I_1\Phi_{PL1} + I_2\Phi_{PL2} + I_3\Phi_{PL3} \quad (4)$$

where I_x is the relative contribution to the total PL intensity (as obtained from the PL-decays) of each emissive species. As previously discussed, τ_2 and τ_3 are similar to previously measured values; we can assume that τ_2 corresponds to a Φ_{PL2} of ~35 %, since the relevant PL-lifetime is similar to the one measured in diluted PDV. Li⊂β-CD water solutions (for which emission is mainly due to the intrachain exciton) [91]. Instead, we can assume τ_3 to correspond to a Φ_{PL3} of ~3 % since the related PL-lifetime is similar to the one measured for PDV.Li films for which the emission is mainly due to aggregate states [110], hence we can calculate a Φ_{PL1} for the decay channel 1(τ_1) of ~52 ± 5 %. From Φ_{PL} and τ we can calculate K_R and K_{NR} for all three decay channels, by using the following set of equations (for $x = 1, 2, 3$):

$$\Phi_{PLx} = \frac{K_{Rx}}{K_{Rx} + K_{NRx}}\,;\; \frac{1}{K_{Rx}} = \frac{\tau_x}{\Phi_{PLx}} \quad (5)$$

Since we do not know Φ_{PL} for PDV.Li⊂β-CD after the photons redistribution takes place in the PhC, we can only calculate K_R and K_{NR} for the reference sample. Nevertheless, the variation of the photonic density of states only affects K_R, leaving K_{NR} unchanged (according to Fermi's golden rule, $K_R(\omega) \propto \frac{2\pi}{\hbar}\rho(\mathbf{r}, \omega)$ [111], in which ρ is the photonic density of states). Therefore, knowing K_{NR} from the reference sample we can calculate K_R from $\tau = \frac{1}{K_R + K_{NR}}$.

Although this is a relatively simple approach, it permits to estimate an increase of K_R of 46 and 24 % at the high-energy PBG edge (437 nm), and a decrease of 31 and 27 % inside the PBG (460 nm) for τ_1 and τ_2, respectively (Table 3). τ_3 is unaffected by the redistribution of the photonic density of states; once again this can be explained by the large K_{NR} (for decay channel "3") that is not modified by the presence of the PhC leaving the modification of K_R too small to be measured.

Table 3 Radiative (K_R) and non-radiative (K_{NR}) rates for PDV.Li⊂β-CD incorporated inside the PhC and in the reference sample

	Decay channel 1 (τ_1)	Intrachain exciton (τ_2)	Aggregate states (τ_3)
437 nm (high-energy edge)			
$K_{R(PhC)}$ s^{-1} ($\times 10^8$)	19.8 ± 2	5.1 ± 0.5	0.10 ± 0.01
$K_{R(Reference)}$ s^{-1} ($\times 10^8$)	13.5 ± 2	4.1 ± 0.4	0.10 ± 0.01
460 nm (PBG)			
$K_{R(PhC}$ s^{-1} ($\times 10^8$)	9.5 ± 0.9	3.0 ± 0.3	0.10 ± 0.01
$K_{R(Reference)}$ s^{-1} ($\times 10^8$)	13.6 ± 2	4.1 ± 0.4	0.10 ± 0.01
K_{NR} s^{-1} ($\times 10^8$)	13.7 ± 2	7.5 ± 0.7	3.5 ± 0.3

All rates were calculated using the model proposed in the text. We include an error of 10 % on the calculated value. Reproduced with permission from [98]

4 Conclusion

In conclusion we have investigated two hybrid-organic photoactive systems. Wavelength and angle dependency of the PL suppression-enhancement has been observed due to the presence of the photonic stop-band. Furthermore, we observed a modification of the emission lifetime inside the stop-band and at its high-energy edge. Such variation of the radiative decay rate is assigned to the modulation of the photonic density of state induced by the photonic crystal that affects the infiltrated polymer.

References

1. Yablonovitch, E.: Phys. Rev. Lett. **58**, 2059 (1987)
2. John, S.: Phys. Rev. Lett. **58**, 2486 (1987)
3. Joannopulos, J.D., Meade, R.D., Win, J.N.: Photonic Crystals: Molding the Flow of the Light. Princeton University Press, Princeton (1995)
4. Noda, S., Chutian, A., Imada, M.: Nature **407**, 608 (2000)
5. Lin, S.Y., Fleming, J.G., Hetherington, D.L., Smith, B.K., Biswas, R., Ho, K.M., Sigalas, M. M., Zubrzycki, W., Kurtz, S.R., Bur, J.: Nature **394**, 251 (1998)
6. Mai, L., Ding, F., Stöferle, T., Knoll, A., Jan Offrein, B., Mahrt, R.F.: Appl. Phys. Lett. **103**, 243305 (2013)
7. Jebali, A., Mahrt, R.F., Moll, N., Erni, D., Bauer, C., Bona, G.-L., Bächtold, W.: J. Appl. Phys. **96**, 3043 (2004)
8. Moll, N., Stöferle, T., Schönenberger, S., Mahrt, R.F.: Opt. Express **17**, 20998 (2009)
9. Kawata, S., Sun, H., Tanaka, T., Takada, K.: Nature **412**, 697 (2001)
10. Maruo, S., Nakamura, O., Kawata, S.: Opt. Lett. **22**, 132 (1997)
11. Moon, G.D., Lee, T.I., Kim, B., Chae, G., Kim, J., Kim, S., Myoung, J.-M., Jeong, U.: ACS Nano **5**, 8600 (2011)
12. Belardini, A., Benedetti, A., Centini, M., Leahu, G., Mura, F., Sennato, S., Sibilia, C., Robbiano, V., Giordano, M.C., Martella, C., Comoretto, D., de Mongeot, F.B.: Adv. Opt. Mater. **2**, 208 (2014)
13. Koenderink, A.F., Johnson, P.M., Lopez, J.F.G., Vos, W.L.: CR Phys. **3**, 67 (2002)
14. Hartsuiker, A., Vos, W.L.: Langmuir **24**, 4670 (2008)
15. Comoretto, D., Grassi, R., Marabelli, F., Andreani, L.C.: Mat. Sci. Eng. C **23**, 61 (2003)
16. Bolognesi, A., Mercogliano, C., Yunus, S., Civardi, M., Comoretto, D., Turturro, A.: Langmuir **21**, 3480 (2005)
17. Johnson, N.P., McComb, D.W., Richel, A., Treble, B.M., Rue, R.M.D.L.: Synth. Met. **116**, 469 (2001)
18. Míguez, H., Meseguer, F., Lopez, C., López-Tejeira, F., Sunchez-Dehesa, J.: Adv. Mater. **13**, 393 (2001)
19. Galisteo-Lopez, J.F., Vos, W.L.: Phys. Rev. E **66**, 036616 (2002)
20. Frezza, L., Patrini, M., Liscidini, M., Comoretto, D.: J. Phys. Chem. C **115**, 19939 (2011)
21. Canazza, G., Scotognella, F., Lanzani, G., Silvestri, S.D., Zavelani-Rossi, M., Comoretto, D.: Laser Phys. Lett. **11**, 035804 (2014)
22. Lehmann, V., Föll, H.: J. Electrochem. Soc. **137**, 653 (1990)
23. Barillaro, G., Nannini, A., Piotto, M.: Sensors Actuators A Phys. **102**, 195 (2002)
24. Bassu, M., Surdo, S., Strambini, L.M., Barillaro, G.: Adv. Funct. Mater. **22**, 1222 (2012)

25. Barillaro, G., Strambini, L.M., Annovazzi-Lodi, V., Merlo, S.: IEEE J. Sel. Top. Quantum Electron. **15**, 1359 (2009)
26. Pacholski, C.: Sensors **13**, 4694 (2013)
27. Cregan, R.F., Mangan, B.J., Knight, J.C., Birks, T.A., Russell, P.S.J., Roberts, P.J., Allan, D.C.: Science **285**, 1537 (1999)
28. Liu, Y., Salemink, H.W.M.: Opt. Express **20**, 19912 (2012)
29. Guldin, S., Hüttner, S., Kolle, M., Welland, M.E., Müller-Buschbaum, P., Friend, R.H., Steiner, U., Tétreault, N.: Nano Lett. **10**, 2303 (2010)
30. Wiesmann, C., Bergenek, K., Linder, N., Schwarz, U.T.: Laser Photonics Rev. **3**, 262 (2009)
31. Tessler, N., Denton, G.J., Friend, R.H.: Nature **382**, 695 (1996)
32. Painter, O., Lee, R.K., Scherer, A., Yariv, A., O'Brien, J.D., Dapkus, P.D., Kim, I.: Science **284**, 1819 (1999)
33. Pavarini, E., Andreani, L.C., Soci, C., Galli, M., Marabelli, F., Comoretto, D.: Phys. Rev. B **72**, 045102 (2005)
34. Barth, M., Gruber, A., Cichos, F.: Phys. Rev. B **72**, 085129 (2005)
35. Samuel, I.D.W., Turnbull, G.A.: Mater. Today **28**, 28 (2004)
36. Samuel, I.D.W., Turnbull, G.A.: Chem. Rev. **107**, 1272 (2007)
37. Mróz, M.M., Sforazzini, G., Zhong, Y., Wong, K.S., Anderson, H.L., Lanzani, G., Cabanillas-Gonzalez, J.: Adv. Mater. **25**, 4347 (2013)
38. Gwinner, M.C., Khodabakhsh, S., Song, M.H., Schweizer, H., Giessen, H., Sirringhaus, H.: Adv. Funct. Mater. **19**, 1360 (2009)
39. Yang, Y., Turnbull, G.A., Samuel, I.D.W.: Appl. Phys. Lett. **92**, 163306 (2008)
40. Mróz, M.M., Perissinotto, S., Virgili, T., Gigli, G., Salerno, M., Frampton, M.J., Sforazzini, G., Anderson, H.L., Lanzani, G.: Appl. Phys. Lett. **95**, 31108 (2009)
41. Chénais, S., Forget, S.: Polym. Int. **61**, 390 (2012)
42. McGehee, M.D., Díaz-García, M.A., Hide, F., Gupta, R., Miller, E.K., Moses, D., Heeger, A. J.: Appl. Phys. Lett. **72**, 1536 (1998)
43. Kallinger, C., Hilmer, M., Haugeneder, A., Perner, M., Spirkl, W., Lemmer, U., Feldmann, J., Scherf, U., Müllen, K., Gombert, A., Wittwer, V.: Adv. Mater. **10**, 920 (1998)
44. Scotognella, F., Monguzzi, A., Cucini, M., Meinardi, F., Comoretto, D., Tubino, R.: Int. J. Photoenergy **2008**, 389034 (2008)
45. Yoon, J., Lee, W., Thomas, E.L.: Nano Lett. **6**, 2211 (2006)
46. Yoshino, K., Tatsuhara, S., Kawagishi, Y., Ozaki, M., Zakhidov, A.A., Vardeny, Z.V.: Appl. Phys. Lett. **74**, 2590 (1999)
47. Yoshino, K., Lee, S.B., Tatsuhara, S., Kawagishi, Y., Ozaki, M., Zakhidov, A.A.: Appl. Phys. Lett. **73**, 3506 (1998)
48. Jin, F., Li, C.-F., Dong, X.-Z., Chen, W.-Q., Duan, X.-M.: Appl. Phys. Lett. **89**, 241101 (2006)
49. Jin, F., Shi, L.-T., Zheng, M.-L., Dong, X.-Z., Chen, S., Zhao, Z.-S., Duan, X.-M.: J. Phys. Chem. C **117**, 9463 (2013)
50. Gottardo, S., Sapienza, R., Garcia, P.D., Blanco, A., Wiersma, D.S., Lopez, C.: Nat. Photonics **2**, 429 (2008)
51. Moll, N., Mahrt, R.F., Bauer, C., Giessen, H., Schnabel, B., Kley, E.B., Scherf, U.: Appl. Phys. Lett. **80**, 734 (2002)
52. Lemmer, U., Heun, S., Mahrt, R.F., Scherf, U., Hopmeier, M., Siegner, U., Go¨bel, E.O., Mu¨llen, K., Ba¨ssler, H.: Chem. Phys. Lett. **240**, 373 (1995)
53. Brédas, J.-L., Cornil, J., Heeger, A.J.: Adv. Mater. **8**, 447 (1996)
54. Segal, M., Baldo, M.A., Holmes, R.J., Forrest, S.R., Soos, Z.G.: Phys. Rev. B **68**, 075211 (2003)
55. Burin, A.L., Ratner, M.A.: J. Phys. Chem. A **104**, 4704 (2000)
56. Coropceanu, V., Cornil, J., da Silva Filho, D.A., Olivier, Y., Silbey, R., Brédas, J.-L.: Chem. Rev. **107**, 926 (2007)

57. Kozlov, V.G., Parthasarathy, G., Burrows, P.E., Khalfin, V.B., Wang, J., Chou, S.Y., Forrest, S.R.: IEEE J. Quantum Electron. **36**, 18 (2000)
58. Cacialli, F., Wilson, J.S., Michels, J.J., Daniel, C., Silva, C., Friend, R.H., Severin, N., Samori, P., Rabe, J.P., O'Connell, M.J., Taylor, P.N., Anderson, H.L.: Nat. Mater. **1**, 160 (2002)
59. Barta, P., Cacialli, F., Friend, R.H., Zagórska, M.: J. Appl. Phys. **84**, 6279 (1998)
60. Gigli, G., Barbarella, G., Favaretto, L., Cacialli, F., Cingolani, R.: Appl. Phys. Lett. **75**, 439 (1999)
61. Frampton, M.J., Anderson, H.L.: Angew. Chem. Int. Ed. **46**, 1028 (2007)
62. Ruminski, A.M., Barillaro, G., Secret, E., Huang, W.D., Potocny, A., Carion, U., Wertans, C., Sailor, M.J.: Adv. Opt. Mater. **1**, 510 (2013)
63. Presti, C.D., Irrera, A., Franzò, G., Crupi, I., Priolo, F., Iacona, F., Di Stefano, G., Piana, A., Sanfilippo, D., Fallica, P.G.: Appl. Phys. Lett. **88**, 033501 (2006)
64. Galli, M., Politi, A., Belotti, M., Gerace, D., Liscidini, M., Patrini, M., Andreani, L.C., Miritello, M., Irrera, A., Priolo, F., Chen, Y.: Appl. Phys. Lett. **88**, 251114 (2006)
65. Lin, V.S.-Y., Motesharei, K., Dancil, K.-P.S., Sailor, M.J., Ghadiri, M.R.: Science **278**, 840 (1997)
66. Ruminski, A.M., Moore, M.M., Sailor, M.J.: Adv. Funct. Mater. **18**, 3418 (2008)
67. Ruminski, A.M., Barillaro, G., Chaffin, C., Sailor, M.J.: Adv. Funct. Mater. **21**, 1511 (2011)
68. Surdo, S., Merlo, S., Carpignano, F., Strambini, L.M., Trono, C., Giannetti, A., Baldini, F., Barillaro, G.: Lab Chip **12**, 4403 (2012)
69. Kilian, K.A., Böcking, T., Gaus, K., Gal, M., Gooding, J.J.: ACS Nano **1**, 355 (2007)
70. Kilian, K.A., Lai, L.M.H., Magenau, A., Cartland, S., Böcking, T., Di Girolamo, N., Gal, M., Gaus, K., Gooding, J.J.: Nano Lett. **9**, 2021 (2009)
71. Tokranova, N.A., Novak, S.W., Castracane, J., Levitsky, I.A.: J. Phys. Chem. C **117**, 22667 (2013)
72. Ciampi, S., Böcking, T., Kilian, K.A., Harper, J.B., Gooding, J.J.: Langmuir **24**, 5888 (2008)
73. Hérino, R.: Mat. Sci. Eng. B. **69–70**, 70 (2000)
74. Harraz, F.A., Salem, M.S., Sakka, T., Ogata, Y.H.: Electrochim. Acta **53**, 3734 (2008)
75. Segal, E., Perelman, L.A., Cunin, F., Di Renzo, F., Devoisselle, J.M., Li, Y.Y., Sailor, M.J.: Adv. Funct. Mater. **17**, 1153 (2007)
76. Vos, W.L., Sprik, R., van Blaaderen, A., Imhof, A., Lagendijk, A., Wegdam, G.H.: Phys. Rev. B **53**, 16231 (1996)
77. Ramsdale, C.M., Greenham, N.C.: J. Phys. D. Appl. Phys. **36**, L29 (2003)
78. Jalkanen, T., Torres-Costa, V., Mäkilä, E., Kaasalainen, M., Koda, R., Sakka, T., Ogata, Y. H., Salonen, J.: ACS Appl. Mater. Interfaces **6**, 2884 (2014)
79. Kim, K., Webster, S., Levi, N., Carroll, D.L., Pinto, M.R., Schanze, K.S.: Langmuir **21**, 5207 (2005)
80. Lazzerini, G.M., Di Stasio, F., Fléchon, C., Caruana, D.J., Cacialli, F.: Appl. Phys. Lett. **99**, 243305 (2011)
81. Lazzerini, G.M., Mian, S., Di Stasio, F., Merari Masillamani, A., Crivillers, N., Reinders, F., Mayor, M., Samorì, P., Cacialli, F.: Appl. Phys. Lett. **101**, 153306 (2012)
82. Lopez, C.: Adv. Mater. **15**, 1679 (2003)
83. Rybin, M.V., Khanikaev, A.B., Inoue, M., Samusev, K.B., Steel, M.J., Yushin, G., Limonov, M.F.: Phys. Rev. Lett. **103**, 4 (2009)
84. Galisteo-Lopez, J.F., Ibisate, M., Sapienza, R., Froufe-Perez, L.S., Blanco, A., Lopez, C.: Adv. Mater. **23**, 30 (2011)
85. Pasquazi, A., Stivala, S., Assanto, G., Amendola, V., Meneghetti, M., Cucini, M., Comoretto, D.: Appl. Phys. Lett. **93**, 3 (2008)
86. Nikolaev, I.S., Lodahl, P., Vos, W.L.: Phys. Rev. A **71**, 10 (2005)
87. Morandi, V., Marabelli, F., Amendola, V., Meneghetti, M., Comoretto, D.: Adv. Funct. Mater. **17**, 2770 (2007)

88. Lodahl, P., van Driel, A.F., Nikolaev, I.S., Irman, A., Overgaag, K., Vanmaekelbergh, D., Vos, W.L.: Nature **430**, 654 (2004)
89. Berti, L., Cucini, M., Di Stasio, F., Comoretto, D., Galli, M., Marabelli, F., Manfredi, N., Marinzi, C., Abbotto, A.: J. Phys. Chem. C **114**, 2403 (2010)
90. McCaughey, B., Costello, C., Wang, D., Hampsey, J.E., Yang, Z., Li, C., Brinker, C.J., Lu, Y.: Adv. Mater. **15**, 1266 (2003)
91. Brovelli, S., Latini, G., Frampton, M.J., McDonnell, S.O., Oddy, F.E., Fenwick, O., Anderson, H.L., Cacialli, F.: Nano Lett. **8**, 4546 (2008)
92. Mroz, M.M., Perissinotto, S., Virgili, T., Gigli, G., Salerno, M., Frampton, M.J., Sforazzini, G., Anderson, H.L., Lanzani, G.: Appl. Phys. Lett. **95**, 3 (2009)
93. Brovelli, S., Virgili, T., Mroz, M.M., Sforazzini, G., Paleari, A., Anderson, H.L., Lanzani, G., Cacialli, F.: Adv. Mater. **22**, 3690 (2010)
94. Brovelli, S., Meinardi, F., Winroth, G., Fenwick, O., Sforazzini, G., Frampton, M.J., Zalewski, L., Levitt, J.A., Marinello, F., Schiavuta, P., Suhling, K., Anderson, H.L., Cacialli, F.: Adv. Funct. Mater. **20**, 272 (2010)
95. Brovelli, S., Cacialli, F.: Small **6**, 2796 (2010)
96. Dimitrov, A.S., Nagayama, K.: Langmuir **12**, 1303 (1996)
97. Di Stasio, F., Cucini, M., Berti, L., Comoretto, D., Abbotto, A., Bellotto, L., Manfredi, N., Marinzi, C.: J. Eur. Opt. Soc. **4**, 7 (2009)
98. Di Stasio, F., Berti, L., McDonnell, S.O., Robbiano, V., Anderson, H.L., Comoretto, D., Cacialli, F.: APL Mater. **1**, 042116 (2013)
99. Di Stasio, F., Berti, L., Burger, M., Marabelli, F., Gardin, S., Dainese, T., Signorini, R., Bozio, R., Comoretto, D.: Phys. Chem. Chem. Phys. **11**, 11515 (2009)
100. C. Karnutsch, C. Pflumm, G. Heliotis, J.C. deMello, D.D.C. Bradley, J. Wang, T. Weimann, V. Haug, C. Gartner, U. Lemmer, Appl. Phys. Lett. **90**, 131104 (2007)
101. F. Di Stasio, M. Cucini, D. Comoretto, unpublished
102. Comoretto, D., Robbiano, V., Canazza, G., Boarino, L., Panzarasa, G., Laus, M., Sparnacci, K.: Polym. Compos. **34**, 1443 (2013)
103. Morandi, V., Marabelli, F., Amendola, V., Meneghetti, M., Comoretto, D.: J. Phys. Chem. C **112**, 6293 (2008)
104. M. Cucini, M. Alloisio, A. Demartini, D. Comoretto, in *Biomimetic and Supramolecular System Research,* ed. by A.H. Lima (Nova Science, New York, 2008), p. 91
105. Kasiouli, S., Di Stasio, F., McDonnell, S.O., Constantinides, C.P., Anderson, H.L., Cacialli, F., Hayes, S.C.: J. Phys. Chem. B **117**, 5737 (2013)
106. M. Cucini, R. Narizzano, D. Comoretto, V. Morandi, F. Marabelli, in *Optical Properties of Artificial Opals Infiltrated with a Porphyrin*. International Conference on Optical Probes of p-conjugated polymers and functional self-assemblies, Turku, 11–15 June 2007
107. Latini, G., Parrott, L.J., Brovelli, S., Frampton, M.J., Anderson, H.L., Cacialli, F.: Adv. Funct. Mater. **19**, 3679 (2009)
108. Bechger, L., Lodahl, P., Vos, W.L.: J. Phys. Chem. B **109**, 9980 (2005)
109. Purcell, E.M.: Phys. Rev. **69**, 681 (1946)
110. Petrozza, A., Brovelli, S., Michels, J.J., Anderson, H.L., Friend, R.H., Silva, C., Cacialli, F.: Adv. Mater. **20**, 3218 (2008)
111. Kubo, S., Fujishima, A., Sato, O., Segawa, H.: J. Phys. Chem. C **113**, 11704 (2009)